Radboud Repository

Radboud University Nijmegen

PDF hosted at the Radboud Repository of the Radboud University Nijmegen

The following full text is a preprint version which may differ from the publisher's version.

For additional information about this publication click this link.
http://hdl.handle.net/2066/117305

Trees and spatial topology change in CDT

J. Ambjørn^{a,b} and *T.G. Budd*^{a}

^{a} The Niels Bohr Institute, Copenhagen University
Blegdamsvej 17, DK-2100 Copenhagen Ø, Denmark.
email: ambjorn@nbi.dk, budd@nbi.dk

^{b} Institute for Mathematics, Astrophysics and Particle Physics (IMAPP)
Radbaud University Nijmegen, Heyendaalseweg 135, 6525 AJ, Nijmegen, The Netherlands

Abstract

Generalized causal dynamical triangulations (generalized CDT) is a model of two-dimensional quantum gravity in which a limited number of spatial topology changes is allowed to occur. We solve the model at the discretized level using bijections between quadrangulations and trees. In the continuum limit (scaling limit) the amplitudes are shown to agree with known formulas and explicit expressions are obtained for loop propagators and two-point functions. It is shown that from a combinatorial point of view generalized CDT can be viewed as the scaling limit of planar maps with a finite number of faces and we determine the distance function on this ensemble of planar maps. Finally, the relation with planar maps is used to illuminate a mysterious identity of certain continuum cylinder amplitudes.

arXiv:1302.1763v1 [hep-th] 7 Feb 2013

1

1 Introduction

Two-dimensional quantum gravity has been an important topic in theoretical physics for a long time. String theory *is* two-dimensional quantum gravity coupled to certain conformal field theories in its simplest perturbative formulation. When the central charge c of a conformal field theory is less than one the models correspond to non-critical string theories, and it is possible to solve certain aspects of the gravity-matter system analytically. Also, for $c < 1$ it is possible to provide a path integral regularization of these quantum theories. In this regularization one performs the integration over 2d geometries by summing over equilateral triangulations (so-called *dynamical triangulations* (DT)), eventually recovering the continuum limit by taking the length ϵ of the links to zero. Remarkably, a class of these regularized theories can be solved analytically, even before $\epsilon \rightarrow 0$, using combinatorial techniques, either by directly counting certain graphs or by using so-called matrix models. The outcome of this has been a beautiful Wilsonian picture where one has universality: the continuum limit is to a large extent independent of the details of the regularization. It does not really matter if the starting point is triangulations or one uses quadrangulations or higher order polygons in an arbitrary combination, as long as the weights of these are positive (see e.g. [2], chapter 4, for a review). Thus one has an infinite dimensional coupling constant space, the coupling constants being the relative weights of various types of polygons, and the critical surface where the continuum limit can be taken is a hyper-surface of finite co-dimension. On this hyper-surface one obtains "pure" 2d Euclidean quantum gravity. If one allows negative weights for some polygons one can flow to new continuum theories describing 2d Euclidean quantum gravity coupled to various conformal matter theories, and if one allows for various "flavors" to be attached to the polygons and a local interaction between these, one can obtain all mininal, rational conformal field theories coupled to 2d Euclidean quantum gravity in the continuum limit.

These 2d discretized models can be generalized to higher dimensions [5, 1]. However it has so far not been possible to find a *continuum limit* which can be viewed as higher dimensional quantum gravity. This failure triggered an attempt to define a new class of regularized models where the sums over the piecewise linear geometries were first carried out in spacetimes with Lorentzian signature and local causality was imposed. This class of piecewise linear geometries was denoted *causal dynamical triangulations* (CDT) [8, 6]. When rotating back to Euclidean signature, one is effectively summing over triangulations where there is a *proper-time foliation*. It seems that this class of models has an interesting continuum limit both in three and four dimensions (for a review see [4]), but until now this has only been investigated using computer simulations (in three dimensions somewhat related models have been looked at analytically). Here we will concentrate on 2d where the regularized model can be solved analytically using combinatorial methods. More specifically we will consider a model known as *generalized CDT*, which interpolates between the CDT and DT models [11, 10]. In the generalized CDT model one starts out with space being connected, i.e. having the

topology of S^1, and as a function of proper time one allows it to split into a finite number of S^1 components.[1] Using recent combinatorial results we will solve the discretized model and show how one can obtain the scaling or continuum limit of the model. Further we will discuss how this limit relates to the standard CDT and DT limits. To simplify the discussion we use a model which at the discretized level is described by quadrangulations, rather than triangulations. (in section 7 we show how the results can be generalized to triangulations).

The rest of the article is organized as follows: in section 2 we review how quadrangulations of the sphere are related to labeled planar trees in the case of DT and to unlabeled planar trees in the case of CDT. In section 3 we show how one can use these trees to study a discrete version of generalized CDT and how to find its scaling limit. A more detailed counting of labeled trees in section 4 allows us to study proper time depences in generalized CDT. In section 5 it is shown that generalized CDT can also be interpreted as a scaling limit of random planar maps for which the number of faces is conditioned to remain finite.

There exists an intriguing identity between certain cylinder amplitudes in the scaling limit, first discussed in the context of DT by Kawai and Ishibashi [29] and later in the context of generalized CDT in [10]. Kawai and Ishabashi related the identities to a Virasoro algebra and an underlying conformal invariance, but in the context of generalized CDT the identities appeared quite mysterious. However, we will show that they are even valid at the discretized level and can be understood as a bijection between sets of quadrangulations defining the cylinder amplitudes in question. This is discussed in section 6.

Finally, in section 7 it is shown how some of the quadrangulation results can be generalized to triangulations.

2 Bijections

2.1 Cori–Vauquelin–Schaeffer bijection

The Cori–Vauquelin–Schaeffer bijection relates quadrangulations of the sphere with a marked vertex to planar trees with a labelling. Let us briefly describe the map and its inverse. For details and proofs we refer the reader to [38, 22, 35].

Given a quadrangulation of the sphere with N faces and a marked vertex, which we call the *origin*, we can label the remaining vertices by their distance to the origin along the edges of the quadrangulation. The set of vertices naturally partitions into those with even respectively odd labels. As a consequence of the faces having an even number of sides, this partition turns the edge graph into a bipartite graph, i.e. vertices with even label only connect to vertices with odd label and vice versa. Hence, each

---

[1]In [23] a *continuous cactus* associated to a metric space was defined, that captures the splitting of space in a rigorous manner. In this formulation a finite number of splittings corresponds to a cactus with a finite number of branches.
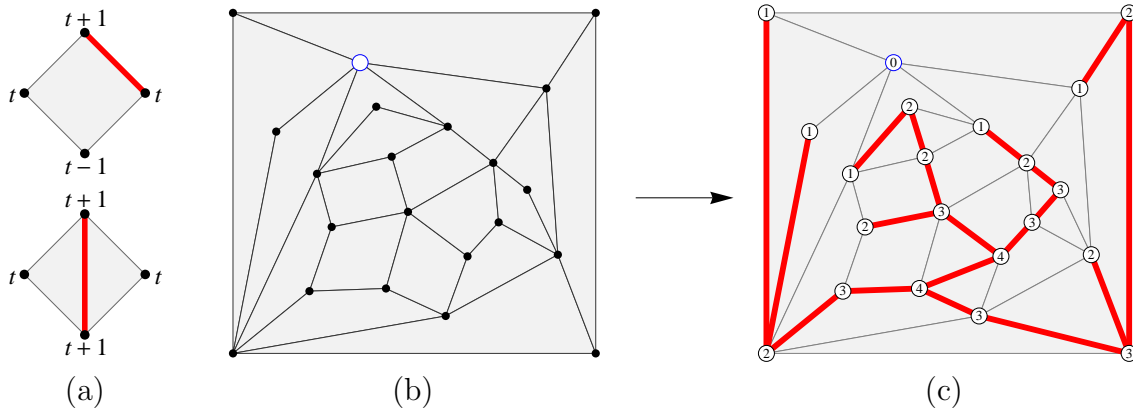
Figure 1: *To every face of the quadrangulation one associates a coloured edge depending on the labeling. The coloured edges combine into a tree connecting all vertices except the origin.*

edge connects vertices with labels differing by exactly one. Taking into account the labeling, two types of faces occur in the quadrangulation, *simple* faces with labels $(t-1, t, t+1, t)$ and *confluent* faces with labels $(t+1, t, t+1, t)$ in cyclic order (see figure 1a and [38, 22]). A graph is drawn on the sphere by coloring the diagonal of each confluent face and the side of each simple face according to the prescription shown in figure 1a. The resulting graph can be shown to be a tree (with N edges) containing all the vertices of the quadrangulation except for the origin. Keeping the labels on the vertices one ends up with a *well-labeled* tree, i.e. a planar tree with positive integers on its vertices, such that at least one vertex is labeled 1 and the labels differ by at most one along its edges.

The quadrangulation can be reconstructed from the well-labeled tree in the following way. First we add by hand a new vertex in the plane, which will be the origin. Then we consider the *contour* of the tree, i.e. the (periodic) sequence of vertices (of length $2N$) encountered when walking around the tree in a clockwise direction. For every entry in the contour we draw a new edge in the plane: if the entry is labeled 1 we connect it to the origin; otherwise we connect it to the first entry following it that has smaller label. Up to deformations there is a unique way of drawing all these edges without crossings. After deleting the tree we are left with the original quadrangulation embedded in the plane.

It is convenient to extend this bijection to the rooted versions of the quadrangulations and trees described above. A *rooted* quadrangulation is a quadrangulation where one of the edges is marked (indicated by a double-sided arrow in figure 2a). Since the edges of the quadrangulation are in 1-to-1 correspondence with the entries in the contour of the tree, we obtain a distinguished entry which we call the *root* of the tree (indicated by a dark arrow in figure 2b). In a rooted tree all edges have a natural orientation, i.e. pointing away from the root. To each edge of the tree we associate a label $+$, 0 or $-$, depending on whether the label increases, remains the same, or
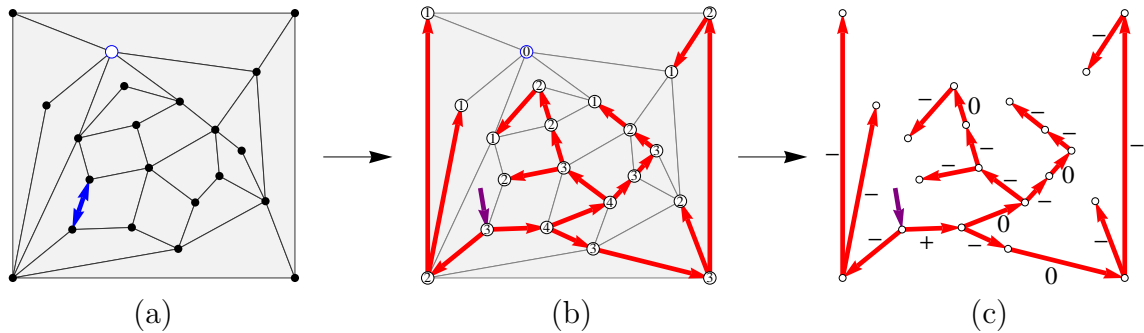
Figure 2: *Rooted quadrangulations with an origin are in bijection with rooted planar trees labelled by +,0,−'s.*

decreases along the edge (see figure 2c). These labels are sufficient to reconstruct the labels on the vertices, since by construction the minimal label on the vertices is fixed to be equal to one. From these constructions it follows that rooted quadrangulations with N faces and an origin are in bijection with rooted planar trees with N edges labeled by +,0,−'s (see [22], Theorem 4).

Notice that this bijection makes the counting of quadrangulations extremely simple. Rooted planar trees with N edges are counted by the Catalan numbers

$$C(N) = \frac{1}{N+1}\binom{2N}{N}, \tag{1}$$

while the number of labelings is simply 3^N. The generating function $z_\ell(g)$ for the number of labeled rooted planar trees, and also for the number of rooted quadrangulations with an origin, is therefore given by

$$z_\ell(g) = \sum_{N=0}^{\infty} 3^N C(N) g^N = \frac{1 - \sqrt{1 - 12g}}{6g}. \tag{2}$$

Since a quadrangulation of the sphere with N faces has $2N$ edges and $N+2$ vertices, the micro-canonical partition function for unmarked quadrangulations is

$$Z(N) = \sum_Q \frac{1}{C_Q} = \frac{3^N}{2N(N+2)} C(N) = \frac{1}{2\sqrt{\pi}} N^{-7/2} 12^N (1 + \mathcal{O}(N^{-1})), \tag{3}$$

where C_Q is the order of the automorphism group of the quadrangulation Q.

2.2 Causal triangulations

A similar bijection between causal triangulations and trees has been used in [36, 32, 27] and earlier in a slightly different form in [26]. In analogy with the quadrangulations in the previous section we can define causal triangulations, which were introduced in
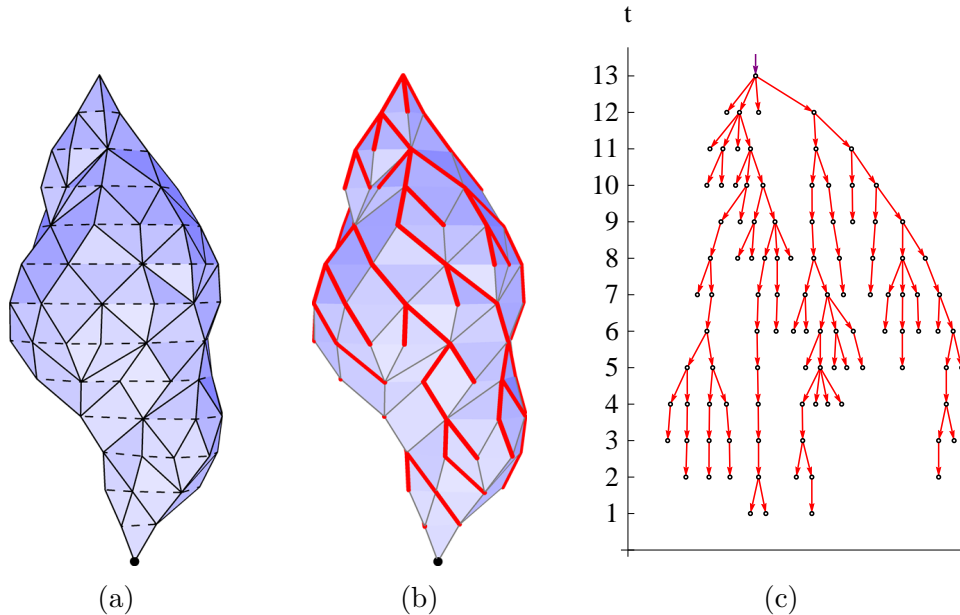
Figure 3: *From (a) causal triangulations to (b) causal quadrangulations to (c) unlabeled planar trees.*

[8], in the following way. Consider a triangulation of the sphere with a marked vertex (the black point in figure 3a), which we call the origin. We interpret the labeling of the vertices that arises from the distance to the origin as a time function, the CDT time. The edges of the triangulation come in two types: *spacelike* edges connecting vertices with identical labels and *timelike* edges connecting vertices with different labels (dashed resp. solid edges in figure 3a). A triangulation with origin is a *causal triangulation* when the graph consisting of only the spacelike edges is a disjoint union of cycles and there is exactly one vertex with maximal label. In other words, the spatial topology as function of CDT time is fixed to be S^1.

Since every triangle in a causal triangulation is bordered by exactly one spacelike edge, there is a canonical pairing of triangles sharing a spacelike edge. By joining all these pairs of triangles into faces, in other words, by deleting the spacelike edges, we end up with a quadrangulation of the sphere (figure 3b). Notice that the removal of the spacelike edges has no effect on the distance labelling, because by construction they connect vertices with indentical labels. Therefore the CDT time on the quadrangulation corresponds exactly to the labeling in the context of the Cori–Vauquelin–Schaeffer bijection. The class of quadrangulations, which we call *causal quadrangulations*, arising from this construction is easily seen to be characterized by the presence of a unique local maximum of the labeling.

If we root the quadrangulation at one of the edges incident to the maximal vertex and apply Schaeffer's prescription, we end up with a rooted planar tree with all edges labeled by −'s (figure 3c). A direct consequence is that rooted causal quadrangulations with N faces, and also rooted causal triangulations with $2N$ triangles, are counted by

6

the Catalan numbers $C(N)$. Their generating function is identical to the generating function $z_u(g)$ of unlabeled trees,

$$z_u(g) = \sum_{N=0}^{\infty} C(N) \, g^N = \frac{1 - \sqrt{1 - 4g}}{2g}.$$ (4)

Later we will see how adding a coupling associated with the labeling allows us to get causal quadrangulations and unrestricted quadrangulations as special cases of a more general model of random trees. But first let us show how one can extract more non-trivial scaling information from these representations by allowing quadrangulations with boundaries.

2.3   Quadrangulations with a boundary

As is shown in [20, 16, 24] the Cori–Vauquelin–Schaeffer bijection extends in a natural way to quadrangulations with a boundary. The simplest such bijection is obtained when we allow the boundary to be of a quite general form, i.e. the boundary is allowed to touch itself and connect disjoint quadrangulations of the disk. An example of such a quadrangulation with a boundary is shown in figure 4a. In fact, this class of geometries includes planar trees as quadrangulations with a finite boundary length but with zero faces. It is convenient to root the quadrangulation by selecting a corner of the exterior face (indicated by an arrow in figure 4a). As before, one of the vertices is marked as the origin, which may lie on the boundary.

Applying Schaeffer's prescription to the distance labeling we obtain a *forest*, i.e. a set of disjoint trees (figure 4b), instead of a single tree in the no-boundary case. Each tree contains at least one boundary vertex. It turns out that there is a distinguished vertex among the boundary vertices which we can use to root the tree. To see this let us orient the boundary of the quadrangulation in a clockwise direction. Then to each boundary edge we can assign a $+$ or $-$ according to whether the label increases or decreases along the edge. It can be shown that each tree contains exactly one boundary vertex that is the end-point of a $+$-edge.

In general this procedure defines a bijection between marked quadrangulations with a boundary of length $2l$ and pairs consisting of a sequence containing l $+$'s and l $-$'s and l independent (possibly empty) rooted labeled trees [16] (see figure 4c). Using this bijection one can easily write down a generating function $w(g, l)$ for the number of quadrangulations with N faces, a marked origin, and a boundary of length $2l$. Since we can arrange the l $+$'s in any way along the boundary of length $2l$, we get

$$w(g, l) = \binom{2l}{l} z_\ell(g)^l,$$ (5)

where $z_\ell(g)$ is the generating function for labeled trees (2). In terms of the boundary
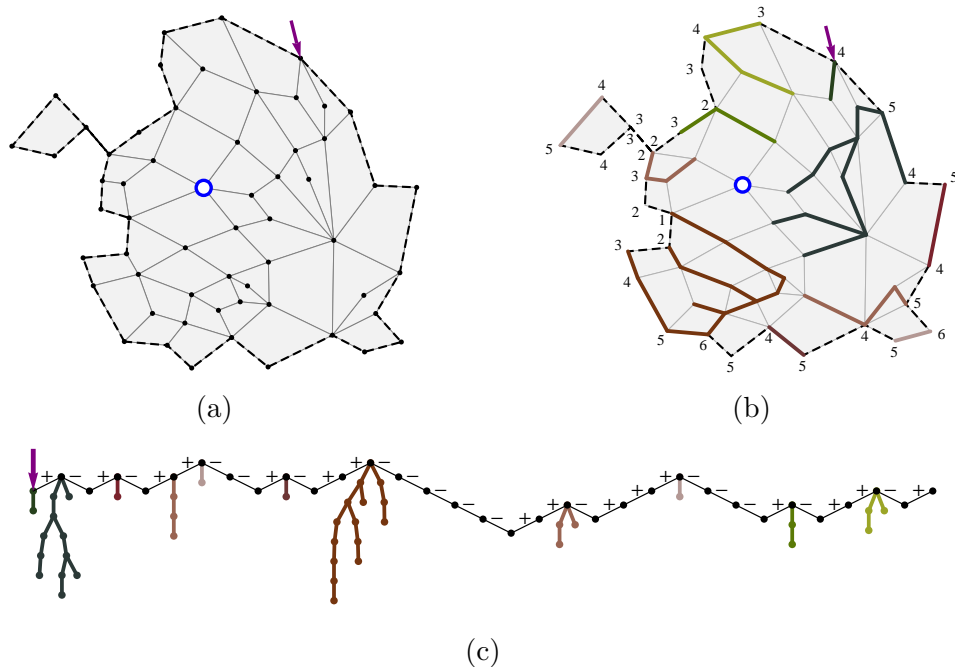
Figure 4: *Quadrangulations with a boundary and an origin are in bijection with sequences of +'s and −'s with a (possibly empty) labeled planar tree growing from each end-point of a +-edge.*

cosmological constant y,

$$w(g, y) = \sum_{l=0}^{\infty} w(g, l) y^l = \frac{1}{\sqrt{1 - 4yz_\ell(g)}}. \tag{6}$$

To obtain the continuum disk-function of 2d gravity we introduce a lattice spacing ϵ, in terms of which we can define a continuum volume $V = N\epsilon^2$ and boundary length $L = l\epsilon$ with canonical dimension. The Laplace transform $W_\Lambda(Y)$ of the continuum disk function $W_V(L)$ is obtained from the discrete disk function $w(g, y)$ by expanding around its critical point at $g_c = 1/12$, $y_c = 1/8$,

$$g = g_c(1 - \Lambda\epsilon^2), \quad y = y_c(1 - Y\epsilon). \tag{7}$$

Plugging these into (6), we obtain

$$w(g, y) = \frac{1}{\sqrt{Y + \sqrt{\Lambda}}} \epsilon^{-1/2}(1 + \mathcal{O}(\epsilon)) = W_\Lambda^{\mathrm{m}}(Y)\epsilon^{-1/2}(1 + \mathcal{O}(\epsilon)), \tag{8}$$

where $W_\Lambda^{\mathrm{m}}(Y)$ is the continuum disk function with a marked point. The familiar unmarked disk function is obtained by integrating W_Λ^{m} with respect to Λ (see also [20], section 4.4),

$$W_\Lambda(Y) = \frac{2}{3}(Y - \frac{1}{2}\sqrt{\Lambda})\sqrt{Y + \sqrt{\Lambda}}. \tag{9}$$

8

More generally one can consider any ensemble of labeled trees with generating function $z(g)$ and compute the correspondig disk function. Provided that the ensemble has a suscepitibility exponent $\gamma = 1/2$, i.e. $z(g)$ is of the form

$$z(g_c) - z(g) \propto (g_c - g)^{1/2}, \tag{10}$$

we can define the continuum tree amplitude through $z(g) = z(g_c)(1 - Z\epsilon)$. The disk function is then simply

$$W_\Lambda^{\mathrm{m}}(Y) = \frac{1}{\sqrt{Y + Z}}. \tag{11}$$

In particular, one can consider the generating function $z_u(g)$ for the ensemble of trees where all labels are $-$'s, related to the causal quadrangulations. The continuum amplitude is simply $Z_u = \sqrt{\Lambda}$, which is exactly the same as for the labeled trees. Contrary to what one might have expected, restricting to causal quadrangulations does not change the continuum disk function.

The explanation is, of course, that this particular disk function is not the one usually considered in the context of CDT. To recover the latter one should consider the disk function where the boundary is restricted to be at constant distance from the origin. In terms of the quadrangulations this is achieved by restricting the labels on the boundary to alternate between two consecutive integers, or, using the bijection, by fixing the boundary sequence to $(+, -, +, -, +, \ldots)$. Since there is only one such sequence, we loose the combinatorial factor in (5) and end up with the disk function

$$w_c(g, y) = \sum_{l=0}^{\infty} w(g, l) y^l = \frac{1}{1 - y\, z(g)}. \tag{12}$$

Its continuum counterpart is

$$W_\Lambda^c(Y) = \frac{1}{Y + Z}, \tag{13}$$

which differs from the unrestricted disk function (11) only by an overall square root. We reproduce the standard CDT disk function[2] by setting $Z = \sqrt{\Lambda}$.

Notice that the overall square root in the marked DT disk function $W_\Lambda^{\mathrm{m}}(Y)$ compared to the CDT disk function $W_\Lambda^c(Y)$ is simply a consequence of the labeling describing a random walk on the boundary. As we will see in section 4, only once the random character of the labeling on the trees is taken into account, will the stark difference in scaling of DT compared to CDT be revealed.

In the next section we will introduce a new partition function for labeled trees, to which we can assign disk functions like above.

---

[2]To get the exact generating function for causal triangulations, one has to glue triangles to all $(-, +)$ pairs on the boundary. The generating function $w_{\mathrm{CDT}}(g, y)$ for the number of causal triangulations with a fixed number of triangles and a fixed boundary length is then $w_{\mathrm{CDT}}(g, y) = w_c(g^2, gy)$.

3 From quadrangulations to generalized CDT

As mentioned earlier causal quadrangulations are characterized by a single local maximum of the labeling, while general quadrangulations can have any number. This suggests a convenient way to interpolate between both models, by assigning a coupling $\mathfrak{g}$ to each local maximum. Then by construction setting $\mathfrak{g} = 0$ will lead to a model of causal quadrangulations and $\mathfrak{g} = 1$ to general quadrangulations. If we interpret the labeling as a time function, we can also view the coupling $\mathfrak{g}$ as a weight for the process of a universe splitting in two, i.e. of spatial topology change.

A model of spatial topology change in continuum CDT was studied in [11, 10, 9] and was referred to as *generalized CDT*. To prevent a proliferation of baby universes in the continuum limit it was found that the coupling $\mathfrak{g}$ should be scaled to zero with the lattice spacing ϵ as $\mathfrak{g} = \mathfrak{g}_s \epsilon^3$. The continuum disk function could be calculated from a graphical consistency relation, leading to

$$W_{\lambda,\mathfrak{g}_s}(X) = \frac{-(X^2 - \lambda) + (X - \alpha)\sqrt{(X + \alpha)^2 - 2\mathfrak{g}_s/\alpha}}{2\mathfrak{g}_s}, \tag{14}$$

where λ is the "effective" CDT cosmological constant (to be discussed in more detail below eq. (22)) and $\alpha = \alpha(\mathfrak{g}_s, \lambda)$ is given by the (largest) solution to

$$\alpha^3 - \lambda\alpha + \mathfrak{g}_s = 0. \tag{15}$$

This equation ensures that $XW_{\lambda,\mathfrak{g}_s}(X) \to 1$ for $X \to \infty$. In the following we will show how we can derive $W_{\lambda,\mathfrak{g}_s}(X)$ by counting quadrangulations with a weight assigned to the local maxima of their labeling and then taking a suitable continuum limit.

However, before we continue, let us introduce a more convenient version of the disk amplitude in (14), for which one of the end points of the baby universes, i.e. one of the local maxima of the time function, is marked. The term of order $\mathfrak{g}_s^n$ in (14) corresponds to surfaces with $n + 1$ such local maxima. Hence we introduce the *cap function*

$$W_{\lambda,\mathfrak{g}_s}^{\mathrm{cap}}(X) = \frac{1}{\sqrt{(X + \alpha)^2 - 2\mathfrak{g}_s/\alpha}}, \tag{16}$$

which satisfies

$$W_{\lambda,\mathfrak{g}_s}^{\mathrm{cap}}(X) = \frac{\partial}{\partial \mathfrak{g}_s}\left(\mathfrak{g}_s W_{\lambda,\mathfrak{g}_s}(X)\right). \tag{17}$$

A vertex with label t is a local maximum on the quadrangulation if all its neighbours, i.e. the vertices connected to it by an edge of the quadrangulation, are labeled $t - 1$, as in figure 5a. Equivalently, its neighbours in the associated well-labeled tree are labeled by t or $t - 1$. Therefore, in terms of the rooted labeled trees we should associate a coupling $\mathfrak{g}$ to every vertex in the tree which has a +- or 0-edge coming in (or no edge in the case of the root vertex) and any number of 0- or $-$-edges going out (figure 5b). Let us denote by $z_0(g) = z_0(g, \mathfrak{g})$ the generating function for such trees. Similarly we
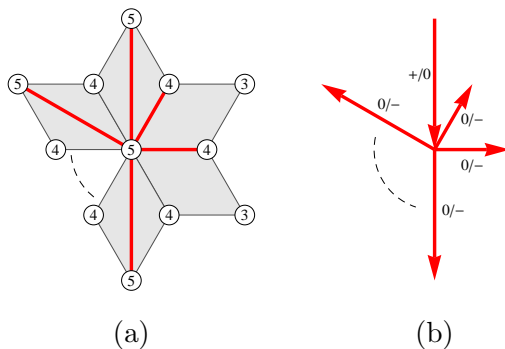
(a) (b)

Figure 5: *A local maximum on the quadrangulation corresponds to a local maximum on the tree, i.e. to a vertex with a +- or 0-edge coming in and any number of 0- or −-edges going out.*

introduce the generating function $z_1(g) = z_1(g, \mathfrak{g})$ with the only difference that we do not assign a coupling $\mathfrak{g}$ to the root vertex, even if there is local maximum there. Both $z_0(g)$ and $z_1(g)$ therefore reduce to the generating function for labeled trees $z_\ell(g)$ from (2) in the case $\mathfrak{g} = 1$. We obtain recurrence relations for $z_0(g)$ and $z_1(g)$ by summing over the number and associated labels of the edges leaving the root,

$$z_1 = \sum_{k=0}^{\infty} (g\, z_1 + g\, z_0 + g\, z_0)^k = \frac{1}{1 - g\, z_1 - 2g\, z_0}$$

$$z_0 = \sum_{k=0}^{\infty} (g\, z_1 + g\, z_0 + g\, z_0)^k + (\mathfrak{g} - 1) \sum_{k=0}^{\infty} (g\, z_1 + g\, z_0)^k \qquad (18)$$

$$= z_1 + \frac{(\mathfrak{g} - 1)}{1 - g\, z_1 - g\, z_0}$$

These combine into a single fourth-order polynomial for $z_1(g)$,

$$3g^2\, z_1^4 - 4g\, z_1^3 + (1 + 2g(1 - 2\mathfrak{g}))z_1^2 - 1 = 0. \qquad (19)$$

The relevant solution, i.e. the one of the form $z_1(g) = 1 + \mathcal{O}(g)$, is given by its smallest positive root. For $\mathfrak{g} = 1$ the solution reduces to (2), while for $\mathfrak{g} = 0$ we get the generating function for unlabeled trees (4), $z_1(g)|_{\mathfrak{g}=0} = z_u(g)$. The latter is not true for $z_0(g)$ since each labeled tree must have at least one local maximum, hence $z_0(g) = 0$ for $\mathfrak{g} = 0$.

In figure 6 we have plotted the solutions for various other fixed values of $\mathfrak{g}$. For each $\mathfrak{g} \geq 0$ there is a critical value $g_c(\mathfrak{g})$ at which $z_1(g)$ becomes non-analytic and at which a continuum limit can be taken. This critical value $g_c(\mathfrak{g})$ is determined by the additional requirement that the derivative $z_1'(g)$ of $z_1(g)$ diverges, which leads to the equation

$$3g_c^2 z_1^4 - 2g_c z_1^3 + 1 = 0. \qquad (20)$$
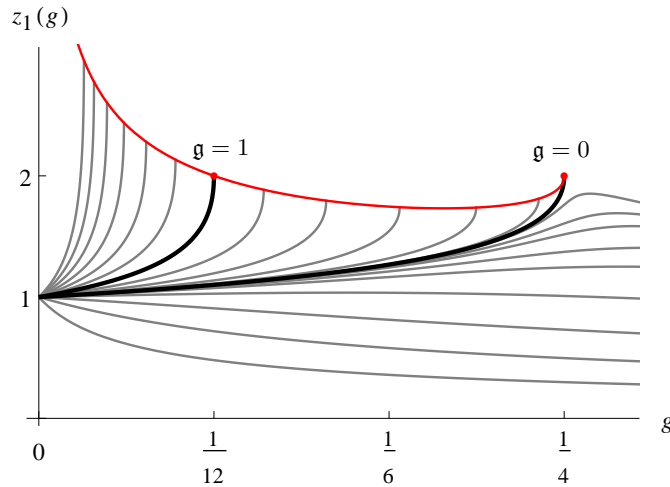
11

Figure 6: *The solution of eq. (19) for various values of $\mathfrak{g}$ as a function of g. For each value of $\mathfrak{g} \leq 0$ the curve ends at the critical line, defined by eq. (20).*

This curve is plotted in red in figure 6.

Unless $\mathfrak{g} = 0$ we obtain an infinite density of baby universes in the continuum limit and presumably we end up in the same universality class as pure DT. This can be seen by calculating the expected number $\langle N_{\max}(\mathfrak{g}) \rangle_N$ of local maxima for fixed large number N of faces, which satisfies

$$\langle N_{\max}(\mathfrak{g}) \rangle_N = \rho(\mathfrak{g})N + \mathcal{O}(N^0), \quad \rho(\mathfrak{g}) = 2\left(\frac{\mathfrak{g}}{2}\right)^{2/3} + \mathcal{O}(\mathfrak{g}), \quad \rho(1) = \frac{1}{2}. \tag{21}$$

If we want to keep $\langle N_{\max}(\mathfrak{g}) \rangle_N$ finite as $N \to \infty$ we should instead scale $\mathfrak{g}$ to zero like $N^{-3/2}$. In the grand-canonical setting this corresponds to scaling $\mathfrak{g} = \mathfrak{g}_s \epsilon^3$ with the lattice spacing ϵ, as observed previously. To take this continuum limit we again expand g around its critical value $g_c(\mathfrak{g}) = 1/4 - 3/4(\mathfrak{g}/2)^{2/3} + \mathcal{O}(\mathfrak{g})$,

$$g = g_c(\mathfrak{g})(1 - \Lambda\epsilon^2) = \frac{1}{4}\left(1 - 3\left(\frac{\mathfrak{g}_s}{2}\right)^{2/3}\epsilon^2 - \Lambda\epsilon^2\right) = \frac{1}{4}(1 - \lambda\epsilon^2), \tag{22}$$

where $\lambda = \Lambda + 3\left(\frac{\mathfrak{g}_s}{2}\right)^{2/3}$ is the "effective" cosmological constant as it was introduced originally in generalized CDT [11]. The original model was formulated directly in the continuum limit and only later, using matrix models, was it understood that λ is actually a sum of contributions coming from a "genuine" cosmological constant Λ related to the "area" of graphs (triangulations, quadrangulations etc.) and a (string) coupling constant $\mathfrak{g}_s$ from splitting off baby universes [3].

Plugging (22) and $z_1(g) = z_1(g_c)(1 - Z_1\epsilon)$ into (19) we obtain the continuum equation

$$Z_1^3 - \lambda Z_1 + \mathfrak{g}_s = 0. \tag{23}$$

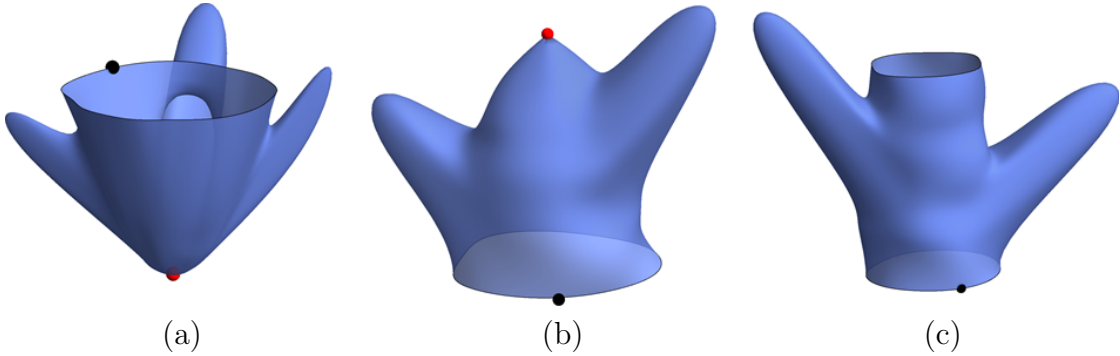Notice that this is exactly equation (15) with $\alpha = Z_1$.

Figure 7: *(a) The cup function $W_{\lambda,\mathfrak{g}_s}^{\mathrm{cup}}(Y)$, (b) the cap function $W_{\lambda,\mathfrak{g}_s}^{\mathrm{cap}}(X)$ and (c) the propagator $G_{\lambda,\mathfrak{g}_s}(X,Y;T)$.*

According to (13) the disk function associated to this ensemble of labeled trees with constant label on the boundary is given by

$$W_{\lambda,\mathfrak{g}_s}^{\mathrm{cup}}(Y) = \frac{1}{Y+Z_1}, \tag{24}$$

which is clearly different from (16). The difference is in the distance function used for the labeling. Here the labeling corresponds to the distance to the marked origin in the disk, while in (16) the distance to the boundary is used and one of the local maxima is marked. We refer to these two disk functions as the *cup function* $W_{\lambda,\mathfrak{g}_s}^{\mathrm{cup}}(Y)$ and the *cap function* $W_{\lambda,\mathfrak{g}_s}^{\mathrm{cap}}(X)$, see figure 7. In order to obtain the cap function we will now study more general time-dependent amplitudes, in particular the two-loop propagator $G_{\lambda,\mathfrak{g}_s}(X,Y;T)$ (figure 7c) and the two-point function $G_{\lambda,\mathfrak{g}_s}(T)$.

4   Time-dependent amplitudes

The simple generating functions discussed in the previous section provide little information about the geometry of the quadrangulations they encode. In order to better understand the geometries and to fully reproduce the results of [11] we need to keep track of the labeling on the trees in more detail. Let us define the generating function $z_0(t) = z_0(t,g,\mathfrak{g})$ for rooted trees with positive integer labels on its vertices and label t on its root. Then $z_0(t) - z_0(t-1)$ is the generating function for well-labeled trees, i.e. labeled trees with minimal label equal to 1, with label t. According to the bijections in section 2, $z_0(t)$ also gives a generating function for the quadrangulations with the furthest end-point of its root edge at most a distance t from the origin, again including a factor of $\mathfrak{g}$ for each local maximum of the distance functions. Likewise, the generating function where this distance is exactly t is $z_0(t) - z_0(t-1)$.

As in the previous section we introduce $z_1(t) = z_1(t,g,\mathfrak{g})$ for which no coupling $\mathfrak{g}$ is assigned to the root vertex. The recurrence relations (18) straightforwardly generalize

13

to

$$z_1(t) = \frac{1}{1 - g\, z_1(t-1) - g\, z_0(t) - g\, z_0(t+1)},$$
$$z_0(t) = z_1(t) + \frac{(\mathfrak{g} - 1)}{1 - g\, z_1(t-1) - g\, z_0(t)}$$

(25)

for $t \geq 1$, subject to the boundary conditions $z_1(0) = 0$ and $z_0(\infty) = z_0$.

Quite remarkably, (25) can be solved analytically using the technique outlined in [17, 25]. Expanding the generating functions around their limits as $t \to \infty$, which are given by the solution z_1 and z_0 to (18), we find after a straightforward but tedious calculation

$$z_1(t) = z_1 \frac{1 - \sigma^t}{1 - \sigma^{t+1}} \frac{1 - (1-\beta)\sigma - \beta\sigma^{t+3}}{1 - (1-\beta)\sigma - \beta\sigma^{t+2}},$$
$$z_0(t) = z_0 \frac{1 - \sigma^t}{1 - (1-\beta)\sigma - \beta\sigma^{t+1}} \frac{(1 - (1-\beta)\sigma)^2 - \beta^2\sigma^{t+3}}{1 - (1-\beta)\sigma - \beta\sigma^{t+2}},$$

(26)

where β and σ are fixed in terms of z_0 and z_1 (hence in terms of g and $\mathfrak{g}$) through

$$g(1+\sigma)(1+\beta\sigma)z_1 - \sigma(1 - 2g\, z_0) = 0,$$
$$(1-\beta)\sigma - g(1+\sigma)z_1 + g(1 - \sigma + 2\beta\sigma)z_0 = 0.$$

(27)

In particular, $\beta = 0$ in the case of CDT ($\mathfrak{g} = 0$) and $\beta = 1$ in the case of DT ($\mathfrak{g} = 1$).

To get to generalized CDT in the continuum limit, the time should be scaled canonically with the lattice spacing, i.e. $t = T/\epsilon$. The scaling $\mathfrak{g} = \mathfrak{g}_s\epsilon^3$ and $g = 1/4(1 - \lambda\epsilon^2)$ implies that the parameters σ and β scale as $\sigma = 1 - 2\Sigma\epsilon$ and $\beta = B\epsilon$. According to (27) the continuum parameters Σ and B are related to λ and $\mathfrak{g}_s$ through

$$\mathfrak{g}_s - 2B(B^2 + 3B\Sigma + 2\Sigma^2) = 0,$$
$$\lambda - 3B^2 - 6B\Sigma - \Sigma^2 = 0.$$

(28)

They can also be expressed in terms of $\mathfrak{g}_s$ and α from equation (15),

$$\Sigma = \frac{1}{2}\sqrt{4\alpha^2 - 2\mathfrak{g}_s/\alpha} \quad \left(= \sqrt{\lambda} - \frac{3\mathfrak{g}_s}{4\lambda} + \mathcal{O}(\mathfrak{g}_s^2)\right),$$
$$B = \alpha - \Sigma.$$

(29)

We also note that, as $\mathfrak{g} \to \infty$, α and Σ grow as

$$\alpha = \left(\frac{\mathfrak{g}_s}{2}\right)^{1/3} + \left(\frac{\Lambda}{3}\right)^{1/2} + O\left(\mathfrak{g}_s^{-1/3}\right), \quad \Sigma = (3\Lambda)^{1/4}\left(\frac{\mathfrak{g}_s}{2}\right)^{1/6} + O\left(\mathfrak{g}_s^{-1/6}\right)$$

(30)

Finally, the solutions (26) scale as $z_1(t) = 2(1 - Z_1(T)\epsilon)$ and $z_0(t) = 2Z_0(T)\epsilon^2$ with

$$Z_1(T) = \alpha + \frac{\Sigma^2}{\sinh(\Sigma T)\left[\Sigma\cosh(\Sigma T) + \alpha\sinh(\Sigma T)\right]},$$
$$Z_0(T) = \frac{\mathfrak{g}_s}{2\alpha}\left(1 - \frac{\Sigma^2}{\left[\Sigma\cosh(\Sigma T) + \alpha\sinh(\Sigma T)\right]^2}\right).$$

(31)

14

Since $z_0(t) - z_0(t-1)$ defines a discrete two-point function, the scaling limit of the two-point function is obtained by differentiating $Z_0(T)$ with respect to T,

$$G_{\lambda,\mathfrak{g}_s}(T) = \frac{dZ_0(T)}{dT} = \Sigma^3 \frac{\mathfrak{g}_s}{\alpha} \frac{\Sigma \sinh \Sigma T + \alpha \cosh \Sigma T}{\left(\Sigma \cosh \Sigma T + \alpha \sinh \Sigma T\right)^3}. \tag{32}$$

In the limit $\mathfrak{g}_s \to 0$ we obtain (up to a factor $\mathfrak{g}_s$ which is convention) the CDT result

$$G_{\lambda,\mathfrak{g}_s=0}(T) \sim e^{-2\sqrt{\Lambda}T}. \tag{33}$$

In the limit $\mathfrak{g}_s \to \infty$ we obtain (again up to a $\mathfrak{g}_s$ factor)

$$G_{\lambda,\mathfrak{g}_s\to\infty}(T) \sim \Lambda^{3/4} \frac{\cosh(\Lambda^{1/4}T')}{\left(\sinh(\Lambda^{1/4}T')\right)^3}, \qquad T' = 3^{1/4} \left(\frac{\mathfrak{g}_s}{2}\right)^{1/6} T. \tag{34}$$

Of course this limit does not exist unless we keep T' finite in the scaling limit rather than T. Thus we are really discussing another scaling limit! Recall that $T \sim t/\epsilon$ and $\mathfrak{g}_s = \mathfrak{g}/\epsilon^3$. Thus a finite T' in the limit $\epsilon \to 0$ can be identified with a scaling limit where $t/\epsilon^{1/2}$ is finite for $\epsilon \to 0$. This is precisely the limit first discussed by Kawai et al. [31] where the *geodesic* distance scales anomalously with respect to volume, leading to the Hausdorff dimension $d_h = 4$ for 2d Euclidean quantum gravity and in the DT ensemble of random graphs. The two-point function (34) was first calculated in [12] (see also [7] and [13] for more general formulas). We note that the "DT limit" $\mathfrak{g}_s \to \infty$ can be identified with the limit $\lambda/(\mathfrak{g}_s/2)^{2/3} \to 3$ from above and is the limit where eq. (23) ceases to have a real positive solution Z_1.

4.1 Boundaries

Let us now turn to the situation where we have boundaries. The cup function $(Y + Z_1(T))^{-1}$ constructed from $Z_1(T)$ takes into account all surfaces with a boundary at constant distance smaller than T from the origin. To get the corresponding cup function with fixed boundary length L one has to take an inverse Laplace transform, leading to

$$e^{-L\,Z_1(T)}. \tag{35}$$

We note that this function can be used to reveal a relation between $Z_0(T)$, $Z_1(T)$ and the disk function $W_{\lambda,\mathfrak{g}_s}(X)$ (which is the cap function without a mark in (14), but which we have not yet determined by the combinatorial methods used in this article). In figure 8 we have depicted the two-point function $Z_0(T)$, which takes into account surfaces with two marked points, i.e. the origin and the root, separated by a distance smaller than T. It seems that this two-point function can be decomposed as follows: first one moves from the origin to the root at a distance $T' \leq T$ from the origin. This root is located on a connected curve of some length L where all points have the same
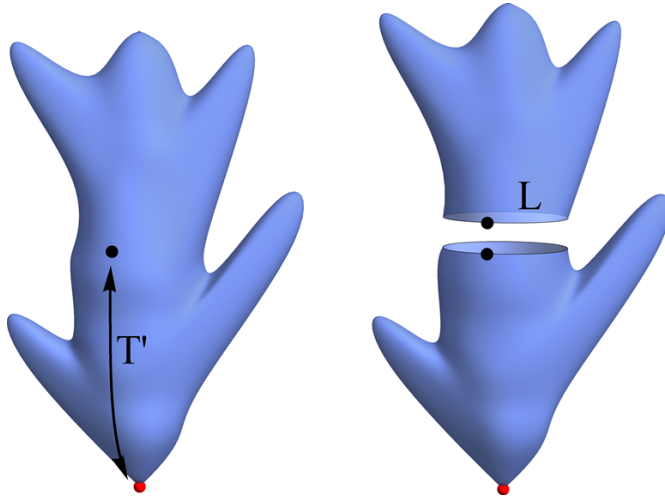
Figure 8: *The two-point function $Z_0(T)$ can be obtained by "closing off" the boundary of a cup function at a fixed distance $T' < T$ from the origin by the disk amplitude.*

distance T' to the origin. Cutting the surface along this curve leads to two disks, both with a mark on the boundary. The bottom disk (see figure 8) has an origin at a fixed distance $T' \leq T$ from the boundary and therefore its amplitude is given by (35). The top disk has no mark in its interior and the labeling is determined by the distance to the boundary of length L, hence its amplitude corresponds to the inverse Laplace transform $W_{\lambda,\mathfrak{g}_s}(L)$ of the disk function $W_{\lambda,\mathfrak{g}_s}(X)$. The two-point function $Z_0(T)$ should therefore be obtained by combining these to disk amplitudes and integrating over L, i.e.

$$Z_0(T) = \mathfrak{g}_s \int_0^\infty dL\, W_{\lambda,\mathfrak{g}_s}(L) e^{-L\,Z_1(T)} = \mathfrak{g}_s W_{\lambda,\mathfrak{g}_s}(Z_1(T)). \qquad (36)$$

We have to add a factor of $\mathfrak{g}_s$ simply because $Z_0(T)$ has a coupling $\mathfrak{g}_s$ for each local maximum, while the term of order $\mathfrak{g}_s^n$ in the disk function $W_{\lambda,\mathfrak{g}_s}(X)$ corresponds to surfaces with $n+1$ local maxima (see the discussion above eq. (16)). Since we have explicitly determined $Z_0(T)$ and $Z_1(T)$ we can verify using (36) that $W_{\lambda,\mathfrak{g}_s}(X)$ is indeed given by formula (14).

The previous analysis leading to the cup function $1/(Y + Z_1(T))$ can be extended to find the *propagator* $G_{\lambda,\mathfrak{g}_s}(X, Y; T)$ for surfaces with two boundaries, an initial boundary with boundary cosmological constant X and a final boundary at a fixed distance T from the initial boundary with boundary cosmological constant Y (see figure 7c). In the discrete setting it is natural to consider quadrangulations with two boundaries, an initial boundary of length $2l_0$ on which the vertices are labeled $(0, 1, 0, 1, \ldots)$ and a final boundary of length $2l_1$ on which they are labeled $(t, t+1, t, t+1, \ldots)$.[3] We can close off the initial boundary by gluing to it a disk constructed from l_0 simple faces, i.e. each of them labeled $(-1, 0, 1, 0)$. This way we obtain a quadrangulation with an

---

[3]Even though quadrangulations with two boundaries of *odd* length exist, we require the boundary lengths to be even to keep them bipartite.

origin labeled -1 (instead of the usual 0) and all faces around the origin conditioned to be simple. If, instead of assigning a weight g to the faces around the origin, we assign to them a weight x, we obtain the generating function for the double-boundary quadrangulations. It is not hard to see that the generating functions $z_{1,x}(t)$ for the corresponding trees satisfy exactly the same equations (25) but with the boundary condition $z_{1,x}(0) = x$ instead of $z_1(0) = 0$.

Since the solution (26) solves (25) for any *real* value $t > 0$ and $z_1(t)$ increases monotonically from 0 at $t = 0$ to z_1 at $t \to \infty$, we immediately find

$$z_{1,x}(t) = z_1\left(t + z_1^{-1}(x)\right), \tag{37}$$

provided $0 \le x < z_1$. This solution has a critical point at $x = z_1$, around which we should expand to get the canonical scaling of the initial boundary length in the continuum limit. Setting $x = 2(1 - X\epsilon)$ leads to $z_{1,x}(t) = 2(1 - Z_{1,X}(T)\epsilon)$ with

$$Z_{1,X}(T) = Z_1(T + Z_1^{-1}(X)). \tag{38}$$

However, one has to keep in mind that this solution is only valid for $X > Z_1 = \alpha$. To get the other part of the solution we have to solve (25) with $\bar{z}_1(t) > z_1$, which can be formally obtained by shifting $t \to t + i\pi/(\log \sigma)$. The corresponding continuum solution $\bar{Z}_1(T)$ is obtained from (31) by shifting $T \to T - i\pi/(2\Sigma)$. This $\bar{Z}_1(T)$ grows monotonically from $\sqrt{2\mathfrak{g}_s/\alpha} - \alpha$ to α and therefore allows us to construct $Z_{1,X}(T)$ for $\sqrt{2\mathfrak{g}_s/\alpha} - \alpha < X < \alpha$. Notice that $X > \sqrt{2\mathfrak{g}_s/\alpha} - \alpha$ is exactly the region where (16) is finite.

Making the replacement $Z_1(T) \to Z_{1,X}(T)$ in the cup function, i.e.

$$\frac{1}{Y + Z_{1,X}(T)}, \tag{39}$$

one almost obtains the sought-after propagator $G_{\lambda,\mathfrak{g}_s}(X,Y;T)$, but not quite. First of all, one should subtract from (39) the cup function $(Y + Z_1(T))^{-1}$, because (39) includes surfaces which do not "reach" the initial boundary, i.e. surfaces which have a final boundary at constant distance smaller than T from a marked point. Secondly, by construction the final boundary is marked, while we want only the initial boundary to be marked (see figure 7c). These are both taken into account by differentiating with respect to X and integrating with respect to Y,

$$G_{\lambda,\mathfrak{g}_s}(X,Y;T) = \int_{\infty}^{Y} dY' \frac{\partial}{\partial X}\left(\frac{1}{Y + Z_{1,X}(T)}\right) = \frac{Z'_{1,X}(T)}{Z'_{1,X}(0)} \frac{1}{Y + Z_{1,X}(T)}. \tag{40}$$

The cap function is obtained from the propagator by integrating over T and taking the final boundary length to zero,

$$W^{\text{cap}}_{\lambda,\mathfrak{g}_s}(X) = \lim_{Y \to \infty} Y \int_0^{\infty} dT\, G_{\lambda,\mathfrak{g}_s}(X,Y;T) = \frac{\alpha - X}{Z'_1(Z_1^{-1}(X))}. \tag{41}$$

17

From (31) it follows that

$$Z'_{1,X}(T) = (\alpha - Z_{1,X}(T))\sqrt{(Z_{1,X}(T) + \alpha)^2 - 2\mathfrak{g}_s/\alpha} =: -\bar{W}(Z_{1,X}(T)), \qquad (42)$$

where we have introduced the notation

$$\bar{W}(X) = (X - \alpha)\sqrt{(X + \alpha)^2 - 2\mathfrak{g}_s/\alpha}, \qquad (43)$$

and thus (41) reproduces exactly (16). Further, (40) shows that the loop propagator satisfies the differential equation

$$\frac{\partial}{\partial T} G_{\lambda,\mathfrak{g}_s}(X, Y; T) = -\frac{\partial}{\partial X}\left(\bar{W}(X)G_{\lambda,\mathfrak{g}_s}(X, Y; T)\right), \qquad (44)$$

since (42) is the characteristic equation for (44) and (40) is thus the solution with initial boundary condition

$$G_{\lambda,\mathfrak{g}_s}(X, Y; T = 0) = \frac{1}{X + Y}, \quad \text{or} \quad \tilde{G}_{\lambda,\mathfrak{g}_s}(L_1, L_2; T = 0) = \delta(L_1 - L_2), \qquad (45)$$

where $\tilde{G}_{\lambda,\mathfrak{g}_s}(L_1, L_2; T)$ is the inverse Laplace transform of $G_{\lambda,\mathfrak{g}_s}(X, Y; T)$.

An alternative route towards the solutions (31) and the propagator (40) is to directly take the continuum limit of the recurrence relations (25). This is done by substituting

$$\begin{aligned} z_1(t + s) &= 2\left(1 + \epsilon(Z_1(T) + s\,\epsilon Z'_1(T))\right) \\ z_0(t + s) &= 2\epsilon^2\left(Z_0(T) + s\,\epsilon Z'_0(T)\right) \end{aligned} \quad s \in \{0, 1, 2, 3\}, \qquad (46)$$

in (25) leading to the differential equations

$$Z'_1(T) = \lambda - Z_1(T)^2 - 2Z_0(T), \qquad (47)$$
$$Z'_0(T) = 2Z_1(T)Z_0(T) - \mathfrak{g}_s. \qquad (48)$$

It can be checked that these equations are solved by (31), but it might be more enlightening to show how they contain all information about the disk function. First we note that the equations imply

$$Z''_1(T) = 2\left(Z_1(T)^3 - \lambda Z_1(T) + \mathfrak{g}_s\right). \qquad (49)$$

Integration and the assumption that $Z_1(T) \to Z_1 = \alpha$ for $T \to \infty$ then implies:

$$Z'_1(T) = -\bar{W}(Z_1(T)), \qquad Z_0(T) = \mathfrak{g}_s W_{\lambda,\mathfrak{g}_s}(Z_1(T)). \qquad (50)$$

where $W_{\lambda,\mathfrak{g}_s}(X)$ is given by (14). While this determines $W_{\lambda,\mathfrak{g}_s}(X)$ algebraically, one has to appeal to figure 8, say, to identify it as the disk function, as done previously.
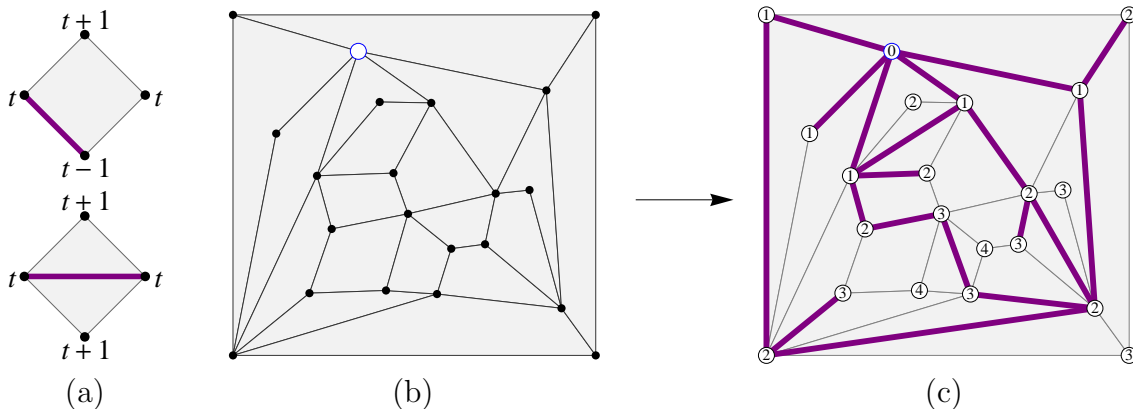
18

Figure 9: *The prescription (a) opposite to Schaeffer's prescription gives a bijection between quadrangulations with an origin (b) and planar maps with an origin (c).*

5 Generalized CDT in terms of planar maps

Above we have seen that quadrangulations with a certain number of local maxima of the distance functions can be encoded in labeled planar trees with the same number of local maxima. As we will demonstrate in this section, instead of labeled trees, another class of mathematical objects can be used to encode the same information, namely *planar maps*.

A *planar map* is an embedding of a connected multigraph, i.e. a connected graph in which loops and multiple edges are allowed, in the sphere without crossing edges. Two planar maps are considered equivalent if they can be continuously deformed into each other and equivalence classes of planar maps can be described purely combinatorically. The connected components of the complement of a planar map in the sphere are topological disks. These components are called the *faces* of the map and the *degree* of a face is the number of edges bounding it. The quadrangulations from section 2.1 form a special class of planar maps, in which each face is restricted to have degree four.

There exists a well-known bijection Φ_0, often referred to as the *trivial bijection* (see e.g. [35]), between quadrangulations with N faces and an origin and planar maps with N edges and a marked vertex. It can be formulated in a very similar way as the Cori–Vauquelin–Schaeffer bijection, namely in terms of the distance labeling from the origin. In stead of applying the Schaeffer's prescription in figure 1a, for each face the diagonal is drawn that connects vertices of even label. In this way all vertices with even label will be part of the planar map, and the vertices with odd label are in one-to-one correspondence with the faces of the map. It can be seen that this planar map with marked origin completely characterizes the quadrangulation.

However, there exists another, inequivalent bijection Φ between quadrangulations Q with N faces and an origin and planar maps with N edges and a marked vertex. Although we expect this bijection to be known, since it is quite similar to the bijection introduce by Miermont in [37] and used in [19], we were unable to find an explicit

reference to it in the literature. Therefore we will describe it here in more detail than the we did for the bijections in section 2.

To obtain this bijection one uses yet another prescription, which is in a sense the exact opposite of Schaeffer's prescription. As shown in figure 9a, it is the Schaeffer's prescription applied to minus the distance labeling. In figure 9c we have shown the result of the coloring for the same quadrangulation as in figure 1. We claim that the resulting embedded graph is a planar map with a number of faces equal to the number $N_{\max}$ of local maxima of the distance function.

The arguments in [22], proposition 1, can be adapted to show that each connected component of the complement of the embedded graph contains at least one local maximum. Indeed, given any such connected component $\mathcal{C}$, one can find a vertex on its boundary[4] that has largest possible label t. There must exist an edge leading away from this vertex and having $\mathcal{C}$ on its left-hand side. This edge ends at a vertex that is labeled either t or $t-1$, but in both cases it can be seen from the prescription in figure 9a that there must be a vertex in the interior of $\mathcal{C}$ with label $t+1$. Hence, $\mathcal{C}$ must contain at least one local maximum and therefore the number of connected components is at most $N_{\max}$.

According to the Euler characteristic for planar graphs we have $V - E + F - C = 1$, where respectively V, E, F, and C are the number of vertices, edges, faces and connected components of the graph. The number of vertices of Q is $N + 2$ and each vertex of Q that is not a local maximum belongs to the graph, therefore $V = N - N_{\max} + 2$. Above we showed that $F \leq N_{\max}$ and by construction we have $E = N$. Then $V - E + F - C = 1$ implies that $C = 1$ and $F = N_{\max}$. Hence $\Phi(Q)$ is connected and therefore a planar map, and its number of faces is $N_{\max}$. Since the origin is not a local maximum it appears as a marked vertex on the planar map.

To show that $Q \to \Phi(Q)$ is a bijection, let us describe its inverse. The special property of the planar map constructed with the prescription in figure 9a is that the labeling is redundant. In fact, if we know the location of the origin, the labeling can be reconstructed simply by considering the distance function along the edges of the map. The reason for this is that each vertex of the quadrangulation that is labeled $t \geq 1$ and is not a local maximum will appear as a first vertex in a face labeled $(t, t+1, t, t-1)$ in a clockwise order. Hence, there will be an edge in the planar map connecting it to a vertex labeled $t-1$. In other words, the label of a vertex that is not the origin is fixed to the minimal label of its neighbours in the planar map plus one. The only such labeling of a planar map where there is a unique vertex labeled 0 is a distance labeling. Actually, this is directly related to the observation in section 3 that a local maximum on the quadrangulation corresponds to a local maximum on the tree. Here the absence of local minima on the quadrangulation, apart from the origin, implies the absence of local minima on the planar map.

If we have the labeling on the planar map we can insert in each face $\mathcal{F}$ a new vertex

---

[4]We do not know a priori that the connected components are topological disks and therefore their boundaries may consist of more than one cycle of edges.

labeled $t_{\mathcal{F}} + 1$, where $t_{\mathcal{F}}$ is the maximal label of the corners of $\mathcal{F}$. Each corner labeled $t_{\mathcal{F}}$ is then connected to this new vertex by an edge. For each other corner labeled t an edge is drawn connecting it to the next corner in the clockwise direction that has label $t + 1$. It can be seen that all the edges thus drawn together make up the original quadrangulation Q. We will not prove the uniqueness of this operation, since it is essentially identical to the proof in [37].

A consequence of the existence of the bijection Φ is that generalized CDT can be regarded as the scaling limit of random planar maps in which the number of faces is kept finite. As a side remark, notice that combining Φ with the trivial bijection gives a bijection $\Phi_0^{-1} \circ \Phi$ of the set of quadrangulations with N faces with an origin onto itself. It maps quadrangulations with $N_{\max}$ local maxima of the distance function to quadrangulations with exactly $N_{\max}$ vertices at odd distance from the origin.

Recall that a rooted quadrangulation is a quadrangulation with a marked (unoriented) edge, while a rooted planar map is a planar map with a corner of one of the faces marked or, equivalently, with a marked oriented edge. The bijection Φ extends easily to the rooted version of the quadrangulations and planar maps, since the the edges of the quadrangulations Q are in 1-to-1 correspondence with the corners of the faces of the planar map $\Phi(Q)$. Each vertex v in Q at distance d from the marked vertex corresponds either to a face of $\Phi(Q)$ or to a vertex in $\Phi(Q)$ at the same distance d from the marked vertex, depending on whether v is a local maximum of the distance function or not. In section 4 we have studied the distribution of distances from the origin in random quadrangulations with a certain number of local maxima. As a byproduct of this analysis we obtain expressions for the distribution of distances in random planar maps as a function of the number of edges and the number of faces.

Recall from section 4 that $z_0(t) - z_0(t-1)$, with $z_0(t)$ as in (26), is the generating function for the number of rooted quadrangulations with N faces and n local maxima and a marked point at distance equal to t from the furthest end of the root edge. Hence, we find the generating function

$$z_t(g, \mathfrak{g}) := z_0(t+1) - z_0(t) = \sum_{N=0}^{\infty} \sum_{n=0}^{N+1} \mathcal{N}_t(N, n) g^N \mathfrak{g}^n \qquad (51)$$

for the number $\mathcal{N}_t(N, n)$ of such quadrangulations with the marked point exactly at distance t from the closest end of the root edge. These quadrangulations are mapped by Φ exactly onto rooted planar maps with N edges, n faces and a marked point at distance t from the root, which are therefore also counted by $z_t(g, \mathfrak{g})$. It is a direct generalization of the generating function $z_{t=0}(g, \mathfrak{g})$ for rooted planar maps with N edges and n faces first derived by Tutte in [39]. On the other hand it generalizes the two-point functions for planar maps derived in [17, 25, 21] of which the simplest versions roughly correspond to $z_t(g, \mathfrak{g} = 1)$. By plugging the solutions to (18) and (27) into (26) one can explicitly compute the coefficients $\mathcal{N}_t(N, n)$. The first few non-zero values of $\mathcal{N}_t(N, n)$ are shown in figure 10 and are checked to agree with a brute-force enumeration of all planar maps up to $N = 5$.

		$t=0$	$t=1$	$t=2$	$t=3$	$t=4$	$t=5$
$N=1$	$n=1$	1	1				
	$n=2$	1					
$N=2$	$n=1$	2	3	1			
	$n=2$	5	5				
	$n=3$	2					
$N=3$	$n=1$	5	9	5	1		
	$n=2$	22	34	10			
	$n=3$	22	22				
	$n=4$	5					
$N=4$	$n=1$	14	28	20	7	1	
	$n=2$	93	175	89	15		
	$n=3$	164	258	70			
	$n=4$	93	93				
	$n=5$	14					
$N=5$	$n=1$	42	90	75	35	9	1
	$n=2$	386	813	546	165	20	
	$n=3$	1030	1993	954	143		
	$n=4$	1030	1640	420			
	$n=5$	386	386				
	$n=6$	42					

Figure 10: *The first few non-zero values of the number $\mathcal{N}_t(N,n)$ of rooted maps with N edges, n faces and a marked point at distance t from the root.*

6 Loop identities

A process was studied in [11, 10] in which two universes merge and the resulting universe disappears into the vacuum. From a two-dimensional perspective, we consider the amplitude for surfaces with two boundary loops of length L_1 and L_2 respectively separated by a geodesic distance D (figure 11). Contrary to the case of the propagator, where all points on the final boundary are required to have a fixed distance to the initial boundary, here we only fix the minimal distance between the boundaries. To get a generalized CDT amplitude, one has to specify the time on the boundaries, which is taken to be constant T_1 and T_2 respectively. In order to get a continuous time function throughout the surface, the boundary times T_1 and T_2 and the distance D have to satisfy the inequality $|T_1 - T_2| \leq D$. The resulting amplitude is denoted by $G_{\lambda,\mathfrak{g}_s}(L_1, L_2; T_1, T_2; D)$.

In [11, 10] it was shown that $G_{\lambda,\mathfrak{g}_s}(L_1, L_2; T_1, T_2; D)$ can be expressed in terms of two propagators and a cap function. A non-trivial calculation showed that, quite remarkably, the amplitude $G_{\lambda,\mathfrak{g}_s}(L_1, L_2; T_1, T_2; D)$ does not depend on T_1 and T_2 at all,

$$G_{\lambda,\mathfrak{g}_s}(L_1, L_2; T_1, T_2; D) = G_{\lambda,\mathfrak{g}_s}(L_1, L_2; D) \quad \text{(provided } |T_1 - T_2| \leq D). \tag{52}$$
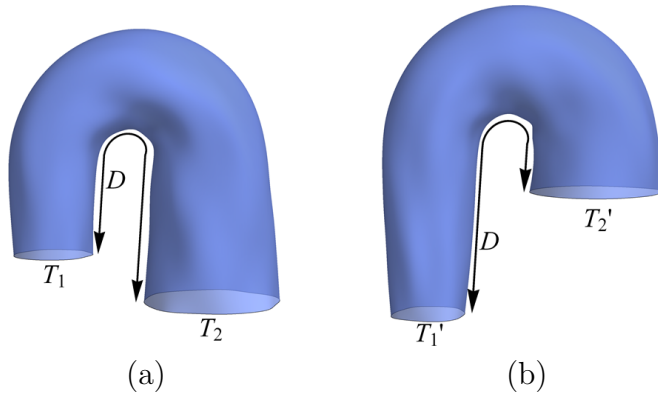
Figure 11: *The two-loop amplitudes $G_{\lambda,\mathfrak{g}_s}(L_1, L_2; T_1, T_2; D)$.*

Even though the same ensemble of surfaces contributes to the loop-loop amplitudes with different initial times, like the ones in figure 11, this is non-trivial because the weight assigned to each surface depends on the number of local maxima of the time functions and therefore on the boundary times.

A similar identity can be derived for Euclidean two-dimensional gravity [13], in which case it can be understood as a consistency relation for the continuum amplitudes. From the discrete point of view, e.g. in terms of the quadrangulations discussed previously, it is clear that such an identity must hold since for $\mathfrak{g} = 1$ the contribution of each quadrangulations is independent of the labeling. In the following we will show that even for $\mathfrak{g} \neq 1$ the discrete two-loop amplitude $\mathcal{G}_{\mathfrak{g}}(l_1, l_2; t_1, t_2; d)$, which is the discrete analogue of $G_{\lambda,\mathfrak{g}_s}(L_1, L_2; T_1, T_2; D)$, is independent of t_1 and t_2. In fact, we will show that for any two pairs (t_1, t_2) and (t'_1, t'_2) there exists a bijection from the set of quadrangulations with two boundaries onto itself, such that a quadrangulation with a number of local maxima with respect to the pair (t_1, t_2) is mapped to a quadrangulation with the same number of local maxima with respect to the pair (t'_1, t'_2). The continuum identity (52) and its discrete analogue are a direct consequence of the existence of such a bijection.

Let us generalize the bijection Φ introduced in the previous section to quadrangulations with two origins instead of one. We consider the set $\mathcal{Q}_d(N)$ of quadrangulations with two marked vertices v_1 and v_2 separated by a distance d along the edges of the quadrangulation. Given a pair of integers (t_1, t_2) satisfying $|t_1 - t_2| < d$ and $t_1 + t_2 + d$ even, one can label the vertices of the quadrangulation in a unique way such that the only local minima occur at the vertices v_i, which are are labeled t_i, and the labels vary by exactly one along the edges. The labeling gives the distance to v_1 shifted by t_1 or the distance to v_2 shifted by t_2, depending on which one is smaller (see [37] for a similar construction). Applying the above construction, i.e. using the prescription in figure 9a, we again get a labeled planar map with a face for each local maximum of the labeling. However, now there are two local minima of the labeling at v_1 and v_2. For the same reason as before, the labeling on the planar map is redundant: it is the

unique labeling with local minima at v_1 and v_2 equal to t_1 and t_2. We claim that this construction gives a bijection

$$\Phi^d_{t_1, t_2} : \mathcal{Q}_d(N) \to \mathcal{M}_d(N) \cup \mathcal{M}_{d-1}(N), \qquad d - |t_1 - t_2| = 2, 4, 6, \ldots, \qquad (53)$$

where $\mathcal{M}_d(N)$ is the set of planar maps with N edges and two marked vertices separated by a distance d.

The only non-straightforward part of the proof is to show that v_1 and v_2 are separated by d or $d - 1$ edges in the planar map, so we will discuss this part in detail. For convenience we assign a *type* to vertices v in the quadrangulation Q according to their distances $d(v, v_i)$ to v_1 and v_2. A vertex v is of type 1 if $d(v, v_1) + t_1 < d(v, v_2) + t_2$, of type 2 if $d(v, v_1) + t_1 > d(v, v_2) + t_2$, and of type 0 in case of equality. For $i = 1, 2$ a type-i vertex v labeled t that is not a local maximum has a distance $t - t_i$ in the planar map to v_i. Due to triangle inequalities all vertices labeled $t < t_{\max} := (t_1 + t_2 + d)/2$ are either of type 1 or type 2. Any path connecting v_1 and v_2 in the planar map must include a vertex labeled $t_{\max} - 1$ of type 1 and of type 2, and therefore its length is at least $d - 1$. Since the distance between v_1 and v_2 in the quadrangulation is d, there must exist at least one vertex $v_{\max}$ with $d(v_0, v_1) + t_1 = d(v, v_2) + t_2 = t_{\max}$, which is the vertex of maximal label on a geodesic connecting v_1 and v_2. Let us consider the cycle of neighbours of $v_{\max}$ in Q in anti-clockwise order. They come in three types: vertices of type 0 labeled $t_{\max} + 1$, vertices of type 1 and type 2 labeled $t_{\max} - 1$. Moreover, at least one vertex of both type 1 and type 2 must occur. Now there are two possibilities for the cycle: either a type-1 vertex is adjacent to a type-2 vertex, or both a type-1 vertex and a type-2 vertex are followed by a type-0 vertex. In the first case the type-1 vertex and the type-2 vertex are opposite corners of a confluent face and are therefore connected by an edge in the planar map. Hence, there is a path of length $d - 1$ connecting v_1 and v_2. In the second case $v_{\max}$ is connected by an edge in the planar map to both a type-1 vertex and a type-2 vertex, resulting in a path of length d.

From the bijection $\Phi^d_{t_1, t_2}$ we can easily construct the desired bijection

$$\Phi^d_{t'_1, t'_2}{}^{-1} \circ \Phi^d_{t_1, t_2} : \mathcal{Q}_d(N) \to \mathcal{Q}_d(N), \quad |t_1 - t_2|, |t'_1 - t'_2| \in \{d - 2, d - 4, \ldots\}, \qquad (54)$$

which maps a quadrangulation with $N_{\max}$ local maxima w.r.t. (t_1, t_2) to a quadrangulation $N_{\max}$ local maxima w.r.t. (t'_1, t'_2).

The bijection (54) can be extended to quadrangulations with two boundaries instead of two marked points by gluing disks to the boundaries as we did for the propagator in section 4. We consider quadrangulations Q with two boundaries, one of length $2l_1$ labeled alternatingly by t_1 and $t_1 + 1$, and another of length $2l_2$ labeled t_2 and $t_2 + 1$. We fix the smallest distance between the points labeled t_1 on the first boundary and the points labeled t_2 on the second boundary to be d, subject to the same inequalities as above, i.e. $d - |t_1 - t_2|$ positive and even. By gluing disks constructed from l_i simple faces to the boundaries, a quadrangulation is obtained with two marked vertices v_i labeled $t_i - 1$ and separated by a distance $d + 2$. The bijection (54) leaves invariant the structure of the quadrangulation in the direct neighbourhood of v_i, and therefore
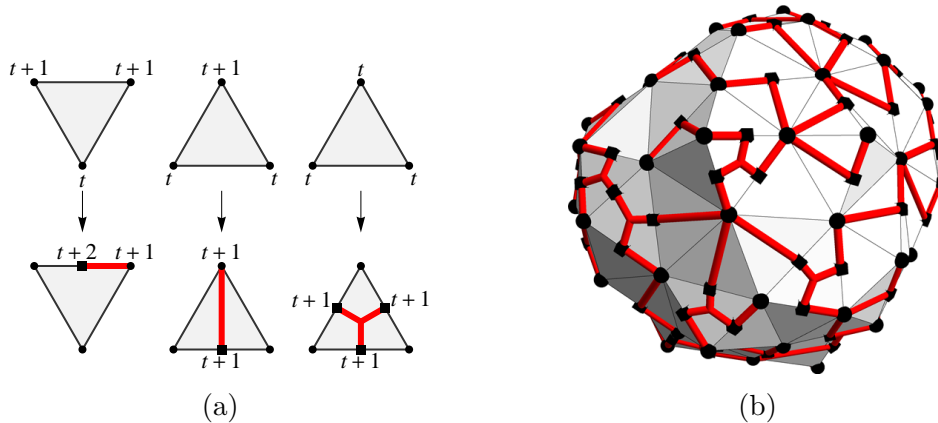
24

Figure 12: *(a) The rules for a "down" triangle, an "up" triangle, and a "flat" triangle respectively. (b) An example of the application of the rules to a triangulation of the sphere.*

the disks can be removed again after the bijection to obtain a quadrangulation with different labels (t_1', t_2') on its boundaries.

7 Triangulations

For the sake of completeness we will show that most constructions in this paper can also be carried out for triangulations. As we will see, the analogues of the bijections described in section 2 are not as simple for triangulations but still manageable. The bijection we will use is a special case of the Bouttier–Di Francesco–Guitter bijection between arbitrary planar maps and *labeled mobiles* introduced in [18]. In a slightly different formulation it was used by Le Gall in [33] to prove that random triangulations and random quadrangulations as metric spaces converge in a quite general way to the same continuum object, known as the *Brownian map*.

The bijection for triangulations can be understood as a special case of the Cori–Vauquelin–Schaeffer bijection for quadrangulations. Given a triangulation of the sphere with N triangles and one vertex marked as the origin, one can label all the vertices according to their distance to the origin along the edges. A new vertex labeled $t+1$ is inserted in the middle of each edge connecting vertices of equal label t. Each triangle with equal labels t, called a *flat* triangle, is subdivided into three faces by connecting each of the three new vertices on its edges to a new vertex labeled $t+2$ in the center of the triangle. The resulting planar map is a quadrangulation labeled by the distance to the origin. It is convenient to keep track of the vertices belong to the triangulation (type 1), the vertices lying on the edges of the triangulation (type 2), and the vertices in the centers of the flat triangles (type 3). The first two types are depicted in figure 12 by disks and squares respectively, while the type-3 vertices correspond to the unmarked intersections.
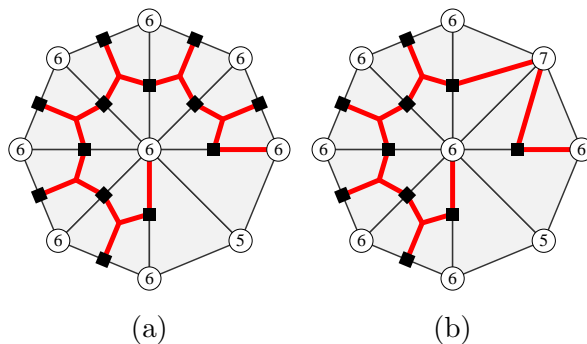
Figure 13: *An example of a vertex that is (a) a local maximum and (b) one that is not.*

The application of Schaeffer's prescription (figure 1a) to the resulting quadrangulation turns out to be equivalent to the prescription in figure 12a for the triangles. Not all quadrangulations arise from triangulations, hence a limited class of labeled trees will appear. Before discussing this class, it is convenient to switch to the rooted versions of the triangulations and trees, like in section 2.1. A triangulation is rooted by distinguishing an edge, which for simplicity we demand to connect vertices of different label.[5] Since this edge appears in the quadrangulation with a vertex of type 1 at its end point with largest label, the tree is naturally rooted at this vertex. From the way the triangles in figure 12a can be glued, it can be seen that the class of rooted, labeled trees satisfies the following rules (see [33]). The root is of type 1. A vertex of type 1 labeled t has zero or more children of type 2 labeled t or $t + 1$. A vertex of type 2 labeled t has either one child of type 1 labeled t or $t - 1$, or two children of type 2 labeled t. Notice that in the latter case we regard the two type-2 vertices of a flat triangle to be directly connected to the other type-2 vertex, instead of keeping track of the type-3 vertex in between.

One would like to identify vertices that are local maxima of the labeling, which in this case means that they have label greater than or equal to their neighbours in the triangulation. In the case of quadrangulations such property of a vertex could be established locally from the labeled tree just by considering the labels of tree edges incident to it. Unfortunately this is not the case for triangulation, as can be seen from the examples in figure 13. Whether or not a vertex is a local maximum may depend on the structure in the tree an arbitrary distance away from that vertex. Assigning couplings to local maxima is an inherently non-local procedure from the point of view of the labeled trees, and therefore quite impractical to treat analytically.

Instead, we will show that one can get a similar model by assigning couplings to saddle-point configurations in the triangulation. In fact, we will introduce two couplings, $\mathfrak{g}_1$ and $\mathfrak{g}_2$, related to two different ways in which saddle points can occur. We assign a coupling $\mathfrak{g}_1$ to each type-1 vertex labeled t that is connected to more than

---

[5]See [33] for the general case where any oriented edge can be used as root.

one type-2 vertex labeled $t+1$. In the triangulation this corresponds to a vertex labeled t for which the labels of its neighbours run from t to $t-1$ and back to t at least twice when walking around the vertex. We also assign a coupling $\mathfrak{g}_2$ to each type-2 vertex labeled t that is not connected to a type-1 vertex labeled $t-1$. This corresponds to an edge labeled (t,t) which is not shared by a *down* triangle (see figure 12a).

Both these configurations are independent and correspond to configurations that are absent in causal triangulations. If we set both couplings to zero and consider rooted, labeled trees for which all edges connecting to the root have constant label, we get exactly causal triangulations rooted at the "top", as in section 2.2. Therefore it makes sense to search for generalized CDT in the continuum limit by scaling the couplings $\mathfrak{g}_1$ and $\mathfrak{g}_2$ to zero.

Let us introduce the generating functions $z_{i,\sigma}(g)$ for trees with a vertex of type $i = 1, 2$ at the root. The label $\sigma = -, 0, +$ indicates whether the tree can be appear as a subtree of a larger tree with an edge of label σ pointing towards the root of the subtree. As can be deduced from the prescription in figure 12a, only four of these are occur, namely $z_{1,-}$, $z_{1,0}$, $z_{2,0}$, and $z_{2,+}$. They satisfy the recurrence relations

$$z_{1,-} = \frac{1-\mathfrak{g}_1}{1-gz_{2,0}} + \frac{\mathfrak{g}_1}{1-gz_{2,+}-gz_{2,0}}, \tag{55}$$

$$z_{1,0} = \frac{1-\mathfrak{g}_1}{1-gz_{2,0}} + gz_{2,+}\frac{1-\mathfrak{g}_1}{(1-gz_{2,0})^2} + \frac{\mathfrak{g}_1}{1-gz_{2,+}-gz_{2,0}}, \tag{56}$$

$$z_{2,0} = g\left(z_{1,-} + \mathfrak{g}_2(z_{1,0} + z_{2,0}^2)\right), \tag{57}$$

$$z_{2,+} = g\left(z_{1,-} + z_{1,0} + z_{2,0}^2\right). \tag{58}$$

If we scale $g = 1/2(1-\lambda\epsilon^2/2)$ and $\mathfrak{g}_i = \mathfrak{g}_{s,i}\epsilon^3$ we find that the generating functions scale as $z_{1,-} = 2(1-Z_{1,-}\epsilon)$, $z_{1,0} = Z_{1,0}/\epsilon$, $z_{2,0} = 1-Z_{2,0}\epsilon$, and $z_{2,+} = Z_{2,+}/\epsilon$, satisfying

$$Z_{1,0} = 2Z_{2,+} = \frac{5}{2Z_{2,0}}, \quad Z_{1,-} = Z_{2,0} \tag{59}$$

$$Z_{2,0}^3 - \lambda Z_{2,0} + \frac{5}{4}\mathfrak{g}_{s,2} = 0. \tag{60}$$

Interestingly, only the coupling $\mathfrak{g}_2$ survives in the continuum limit and produces the generalized CDT coupling $\mathfrak{g}_s$ up to a factor of $5/4$.[6]

The cup function $w(g, y)$ with a constant distance between the boundary and the origin is obtained simply by combining independent trees generated by $z_{2,0}$,

$$w(g, y) = \sum_{l=0}^{\infty} z_{2,0}(g)^l y^l = \frac{1}{1 - y\, z_{2,0}(g)}. \tag{61}$$

Taking the continuum limit of this expression, we arrive at the same result as for quadrangulations (24) with Z_1 replaced by $Z_{2,0}$, which obeys the same equation (60).

---

[6]This slightly awkward factor of $5/4$ can be seen to be due to the presence of flat triangles for small but non-zero $\mathfrak{g}_{s,2}$. If one assigns yet another coupling $\mathfrak{g}_3$ to each flat triangle, which amounts to inserting $\mathfrak{g}_3$ in front of the $z_{2,0}^2$-terms in (57) and (58), and one scales $\mathfrak{g}_3$ to zero at least linearly in ϵ, the factor of $5/4$ will disappear and we get exactly $\mathfrak{g}_{s,2} = \mathfrak{g}_s$.

8 Discussion and conclusions

The model of two-dimensional quantum gravity denoted generalized causal dynamical triangulations was originally introduced as a continuum model of geometries. The equations which determined the disk function and the two-loop function were found from simple consistency relations which had to be satisfied for the ensemble of geometries in question. Only afterwards an actual realization of this ensemble in terms of discrete triangulations was studied, from which a scaling limit could be found by taking the link length to zero, but no detailed analysis in terms of distance functions on the graphs was performed. The purpose of this article has been to present such an analysis, using the powerful technique of labeled trees and their relation to quadrangulations. Quite surprisingly the distance function can be found explicitly at the discretized level for the set of quadrangulations which in a natural way can be used to define generalized CDT. Equally nice, this set of quadrangulations can be mapped onto the set of planar maps with a finite number of faces. Thus we have shown that this set of planar maps has a non-trivial scaling limit and we have found the distance function for this set of maps.

This result should be compared with the results of [34] (see also [30]), where random planar maps are studied with non-trivial weights on the sizes of the faces. By choosing different asymptotic laws for these weights, it was shown that different continuum limits are obtained with Hausdorff dimensions anywhere between 2 and 4. In the context of CDT the sizes of faces are interpreted as (spacetime) volumes of baby universes. It would be interesting to see whether putting weights on the volumes of baby universes leads to continuum limits that continuously interpolate between DT and CDT, and if such weights can be given an interpretation in terms of continuum physics.

Recently it has been shown that one can obtain new scaling relations in the generalized CDT ensemble of graphs if one combines triangles with quadrangles with negative weights ([3] and [14, 15]). This is very similar to the now "classical" situation for the DT ensemble where a similar combination of weights for triangles and quadrangles allowed one to obtain a scaling limit different from the standard DT limit as well as a different distance function ([28] and [17]). It should be possible to use the techniques developed in [17] also for the generalized CDT ensemble, and calculate a distance function for planar maps with a finite number of faces.

Acknowledgments

References

[1] M. Agishtein and A. Migdal. Simulations of four-dimensional simplicial quantum gravity as dynamical triangulation. *Modern Physics Letters A*, 07(12):1039–1061, Apr. 1992.

[2] J. Ambjørn, B. Durhuus, and T. Jonsson. *Quantum geometry : A Statistical field theory approach.* Cambridge Monographs on Mathematical Physics. Cambridge University Press, Cambridge, England, 1997.

[3] J. Ambjørn, L. Glaser, A. Görlich, and Y. Sato. New multicritical matrix models and multicritical 2d CDT. *Physics Letters B*, 712(1-2):109–114, May 2012, arXiv:1202.4435.

[4] J. Ambjørn, A. Görlich, J. Jurkiewicz, and R. Loll. Nonperturbative quantum gravity. *Physics Reports*, 519(4-5):127–210, Oct. 2012, arXiv:1203.3591.

[5] J. Ambjørn and J. Jurkiewicz. Four-dimensional simplicial quantum gravity. *Physics Letters B*, 278(1-2):42–50, Mar. 1992.

[6] J. Ambjørn, J. Jurkiewicz, and R. Loll. Dynamically triangulating Lorentzian quantum gravity. *Nuclear Physics B*, 610(1-2):347–382, Sept. 2001, hep-th/0105267.

[7] J. Ambjørn, J. Jurkiewicz, and Y. Watabiki. On the fractal structure of two-dimensional quantum gravity. *Nuclear Physics B*, 454(1-2):313–342, Nov. 1995, hep-lat/9507014.

[8] J. Ambjørn and R. Loll. Non-perturbative lorentzian quantum gravity, causality and topology change. *Nuclear Physics B*, 536(1-2):407–434, Dec. 1998, hep-th/9805108.

[9] J. Ambjørn, R. Loll, Y. Watabiki, W. Westra, and S. Zohren. A matrix model for 2D quantum gravity defined by causal dynamical triangulations. *Physics Letters B*, 665(4):252–256, July 2008, arXiv:0804.0252.

[10] J. Ambjørn, R. Loll, Y. Watabiki, W. Westra, and S. Zohren. A string field theory based on causal dynamical triangulations. *Journal of High Energy Physics*, 2008(05):032–032, May 2008, arXiv:0802.0719.

[11] J. Ambjørn, R. Loll, W. Westra, and S. Zohren. Putting a cap on causality violations in causal dynamical triangulations. *Journal of High Energy Physics*, 2007(12):017–017, Dec. 2007, arXiv:0709.2784.

[12] J. Ambjørn and Y. Watabiki. Scaling in quantum gravity. *Nuclear Physics B*, 445(1):129–142, July 1995, hep-th/9501049.

[13] H. Aoki, H. Kawai, N. Jun, and A. Tsuchiya. Operator product expansion in two-dimensional quantum gravity. *Nuclear Physics B*, 474(2):512–528, Aug. 1996, hep-th/9511117.

[14] M. R. Atkin and S. Zohren. An analytical analysis of CDT coupled to dimer-like matter. *Physics Letters B*, 712(4-5):445–450, June 2012, arXiv:1202.4322.

[15] M. R. Atkin and S. Zohren. On the quantum geometry of multi-critical CDT. *Journal of High Energy Physics*, 2012(11):1–15, Nov. 2012, arXiv:1203.5034.

[16] J. Bettinelli. Scaling limit of random planar quadrangulations with a boundary. Nov. 2011, arXiv:1111.7227.

[17] J. Bouttier, P. Di Francesco, and E. Guitter. Geodesic distance in planar graphs. *Nuclear Physics B*, 663(3):535–567, July 2003, cond-mat/0303272.

[18] J. Bouttier, P. Di Francesco, and E. Guitter. Planar maps as labeled mobiles. *Elec. Jour. of Combinatorics*, 11:R69, May 2004, math/0405099.

[19] J. Bouttier and E. Guitter. The three-point function of planar quadrangulations. *Journal of Statistical Mechanics: Theory and Experiment*, 2008(07):P07020, July 2008, arXiv:0805.2355.

[20] J. Bouttier and E. Guitter. Distance statistics in quadrangulations with a boundary, or with a self-avoiding loop. *Journal of Physics A: Mathematical and Theoretical*, 42(46):465208, Nov. 2009, arXiv:0906.4892.

[21] J. Bouttier and E. Guitter. Planar maps and continued fractions. *Communications in Mathematical Physics*, 309(3):623–662, Feb. 2012, arXiv:1007.0419.

[22] P. Chassaing and G. Schaeffer. Random planar lattices and integrated superBrownian excursion. *Probability Theory and Related Fields*, 128(2):161–212, Feb. 2004, math/0205226.

[23] N. Curien, J.-F. L. Gall, and G. Miermont. The Brownian cactus I. scaling limits of discrete cactuses. Feb. 2011, arXiv:1102.4177.

[24] N. Curien and G. Miermont. Uniform infinite planar quadrangulations with a boundary. Feb. 2012, arXiv:1202.5452.

[25] P. Di Francesco. Geodesic distance in planar graphs: An integrable approach. *The Ramanujan Journal*, 10(2):153–186, June 2005, arXiv:math/0506543.

[26] P. Di Francesco, E. Guitter, and C. Kristjansen. Integrable 2D Lorentzian gravity and random walks. *Nuclear Physics B*, 567(3):515–553, Feb. 2000, hep-th/9907084.

[27] B. Durhuus, T. Jonsson, and J. F. Wheater. On the spectral dimension of causal triangulations. *Journal of Statistical Physics*, 139(5):859–881, June 2010, arXiv:0908.3643.

[28] S. S. Gubser and I. R. Klebanov. Scaling functions for baby universes in two-dimensional quantum gravity. *Nuclear Physics B*, 416(3):827–849, Apr. 1994, hep-th/9310098.

[29] N. Ishibashi and H. Kawai. String field theory of $c \leq 1$ noncritical strings. *Physics Letters B*, 322(1-2):67–78, Feb. 1994, hep-th/9312047.

[30] S. Janson and S. O. Stefansson. Scaling limits of random planar maps with a unique large face. Dec. 2012, arxiv:1212.5072.

[31] H. Kawai, N. Kawamoto, T. Mogami, and Y. Watabiki. Transfer matrix formalism for two-dimensional quantum gravity and fractal structures of space-time. *Physics Letters B*, 306(1-2):19–26, May 1993, hep-th/9302133.

[32] M. Krikun and A. Yambartsev. Phase transition for the Ising model on the critical Lorentzian triangulation. *Journal of Statistical Physics*, 148(3):422–439, Aug. 2012, arXiv:0810.2182.

[33] J.-F. Le Gall. Uniqueness and universality of the Brownian map. May 2011, arXiv:1105.4842.

[34] J.-F. Le Gall and G. Miermont. Scaling limits of random planar maps with large faces. *The Annals of Probability*, 39(1):1–69, Jan. 2011, arXiv:0907.3262. Zentralblatt MATH identifier: 1204.05088; Mathematical Reviews number (MathSciNet): MR2778796.

[35] J.-F. Le Gall and G. Miermont. Scaling limits of random trees and planar maps. Jan. 2011, arXiv:1101.4856.

[36] V. Malyshev, A. Yambartsev, and A. Zamyatin. Two-dimensional Lorentzian models. *Mosc. Math. J.*, 1(3):439–456, 2001.

[37] G. Miermont. Tessellations of random maps of arbitrary genus. *Annales scientifiques de l'Ecole normale supérieure*, 42(5):725–781, 2009, arXiv:0712.3688.

[38] G. Schaeffer. *Conjugaison d'arbres et cartes combinatoires aleatoires*. PhD thesis, L'Université Bordeaux, 1998.

[39] W. T. Tutte. On the enumeration of planar maps. *Bull. Amer. Math. Soc.*, 74(1):64–74, 1968.